Journal of Materials Science & Technology 79 (2021) 141–146

Contents lists available at ScienceDirect

Journal of Materials Science & Technology

journal homepage: www.jmst.org

Letter

Novel long laminar plasma sprayed hybrid structure thermal barrier coatings for high-temperature anti-sintering and volcanic ash corrosion resistance

1. Introduction

The artificial - designed segmentation cracks in the ceramic layer of the thermal barrier coatings is an excellent choice by using the atmospheric plasma spray (APS) method under a low cost on the applications of aircraft engines or gas turbine engines. The residual thermal stress energy of the coatings with a certain inter-space of vertical cracks during the thermal cycling test is released through the cracks. The coating with vertical cracks was found out to be superior to other coatings with conventional lamellar structure [1]. This process by using the atmospheric plasma spray method usually deposited a dense layer of YSZ (usual thickness of 0.5–1.5 mm) and heating the substrate over 773 K with an auxiliary device previously, even for a complex curved surface of the vanes.

Furthermore, YSZ coatings with dense vertical cracks can also be deposited by using the suspension plasma spray (SPS) method [2]. This process was prepared by using the nano-sized feed powders (e.g. 0.1−1 μm) that were dissolved in water, ethanol or ethyl acetate and also with an auxiliary heating device of the substrate during the whole process [13,14]. Fine void networks at the inter-space of the vertical cracks of coatings were enhanced the phonon scattering and leaded a low thermal conductivity than other coatings [3,4]. However, the deposition rate by using the SPS method do not exceed than one third of the deposition rate of APS method [5,6].

Therefore, both of the current plasma spray processes are focused on the increase of the substrate temperature and liquid splat temperature in order to obtain vertical cracks at the cross-section of the coatings. However, both using the axial injection way or the radial injection way of the feed powders inside or out of the plasma torch, the spray distance is usually in the range of 30 mm–180 mm for the APS and SPS process. Especially, the maximum spraying distance is about 200−250 mm by using a high energy Triplex Plasma Torch [7]. A more short spray distance of 35−80 mm is employed in the SPS process. In these conditions, the lengths of the plasma jet from the non-transferred arc plasma torch are not exceeded 250 mm in an atmospheric environment whatever using nitrogen, helium, argon or these mixture gases (total gas flow rate >25 standard liter per minute) [8]. A large temperature gradient (>200 K mm^{-1}) is existed in these plasma jets in an atmospheric environment [8,9]. Thus, it cannot be used to preciously control the substrate temperature during the deposition.

Moreover, the particle velocity and temperature were simultaneously increased with the increase of output power of the plasma torches basing on the consideration of deposition rate. However, the length of the plasma jet is not apparently increased as the increasing of the output power of plasma torch in the range from 30 kW to 100 kW. The particle temperature is not apparently increased as a short flight time in the plasma jet [10]. In addition, an auxiliary heating part that is designed on the size of the substrate must heat over 773 K before and during the deposition.

An alternative type of the plasma jet in the atmospheric environment is the laminar plasma jet or quasi-laminar plasma jet, which generate by a novel non-transferred arc plasma torch since 1995 [11]. Until now, the maximum length of the plasma jet in the atmospheric environment is about 1000 mm. The output power of this type of plasma torches ranges from 0.9 kW to 70 kW by using argon, hydrogen, nitrogen or mixtures gases at different conditions [12]. The long laminar plasma jet can effectively reduce turbulent cold gas entrainment and the rapid axial attenuation of the jet temperature and velocity [13]. This method may provide a super-long particle flight time for the atmospheric plasma spray process [14,15].

Therefore, this paper investigates a YSZ coating with high density vertical cracks by using a long, silent and stable laminar plasma jet in the ambient air. Microstructures and high-temperature performances of the YZS coating were demonstrated in the following sections.

2. Experiments and methods

Experiments were preformed on a newly developed laminar plasma spray system by using 70 % nitrogen and 30 % argon at a total gas flow rate of 9 SLPM as it is shown in Fig. 1. A very focused deposition position was found when the laminar plasma jet impinges on the substrate (Fig. 1(b)). The powders did not fly around during the deposition [9,12]. It can be used to heating and controlling the substrate temperature through spraying distance, torch moving interval and velocity. The output power of the plasma torch is about 25.4 kW at a current of 160 A [11,15].

The feed material is 8 % yttria stabilized zirconia powder (Metco 204 B-NS, −75 ~ +39 μm, Sulzer Metco, Westbury, USA) in Fig. 1(d). The plasma torch moving interval and velocity in a plane substrate is 4 mm and 0.5 m s^{-1}, respectively. The spraying distance is chosen as 270 mm. The thermal diffusivities of the coating after thermal exposure were measured using a laser-flash apparatus (Netzsch, LFA-427, Germany) [16]. Microhardness Knoop and Vickers indentations were used to measure the elasticity modulus and hardness on the cross-sections of the coating using the HXZ-1000 microhardness indenter [17]. The top surface roughness of the coating was measured by using the Keyence color 3D laser scanning microscope (VK-9700, violet laser). The microstructure observations of coatings used the scanning electron microscope (SEM VEGA II, TESCAN, Czech), including the top surfaces, cross sections and fracture surfaces. The samples for Electron Back-Scattered Diffraction (EBSD) investigations were performed on the cross-section of the coating under an acceleration voltage of 20 kV with a step size of 100

https://doi.org/10.1016/j.jmst.2020.12.002

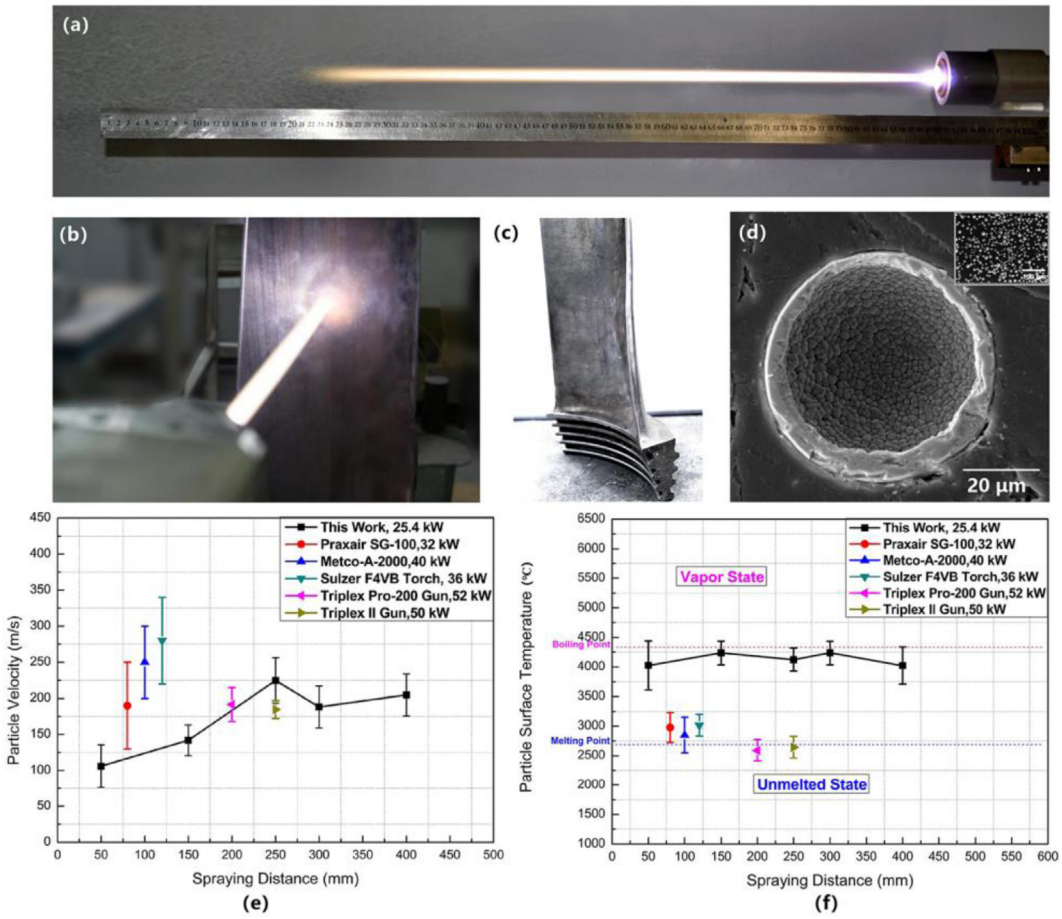

Fig. 1. Photos of the laminar plasma jet in the atmospheric environment (a); the laminar plasma jet impinges on the substrate (b); the used airfoil substrate in (c) and the cross-section of a feed YSZ powder in the experiment (d); experimental measured particle velocity (e) and surface temperature (f) at different spraying distances that compared with other results.

nm. Image quality (IQ) maps, inverse pole figure maps (IPF) and colorcoded grain size distribution maps were used in this paper.

CMAS powders (from sand, debris, fly ash, or volcanic ash) of 33 mol% CaO, 9 mol% MgO, 13 mol% Al_2O_3 and 45 mol% SiO_2 were prepared to investigate high temperature corrosion on the surface of ceramic coatings in three different experiments. The contact angle of CMAS bulk materials on the surface of the coating, CMAS high temperature exposure at 1523 K for 24 h on the surface of the coating and molten CMAS droplets impinging on the thermal barrier coating were studied respectively.

3. Results and discussion

The widely used DPV-2000 Particle Diagnostics System (Technar., Ltd, DVP-2000, Canada) was used in-situ measurement when the particles flowing in the laminar plasma jet at different spraying distances (from 50 mm to 400 mm). The maximum velocity and temperature of the plasma gas at the nozzle exit of the plasma torch by computational fluid dynamics method is about 1500 m s^{-1} and 17000 K [18], respectively. The particle velocity in this work rapidly increased in the range from 50 mm to 250 mm (Fig. 1(e)). The maximum velocity of the particles at the spraying distance of 250 mm is 224.7 m s^{-1}. Then, the particle velocity decreased slightly up to the spraying distance of 400 mm. The distributions of particle surface temperature in the range from 50 mm to 400 mm are all higher than other results in Fig. 1(f) and Table 1. The particle surface temperature in this work is very close to the boiling point of the YSZ materials. Therefore, the YSZ particles flow through a long distance after injection at the nozzle exit when the laminar plasma torch operate in a lower output power and gas flow rate comparing with other APS methods.

The microstructures of the as-sprayed coating were shown in Fig. 2. The apparently vertical cracks from the top to the bottom of the coating were found as a minimum density of 4 per millimeter from the polished cross-section whatever for the as-spray fresh coating (Fig. 2(a)) or for the coating after thermal exposure of 48 h (Fig. 2(b)) and 100 h (Fig. 2(c)) at 1473 K. A mass of multi-islands protrusions were distributed uniformly from the observation on the top surface of the coating in Fig. 2(d). The crack networks were generated around the inter-space of each two island protrusions and connected with the vertical cracks at the cross-section of the coating (Fig. 2(e)). Further, the top of an island protrusion featured as plenty of nano-agglomerated villous structures (Fig. 2(f)). Laser scanning top surface microstructures were shown in Fig. 2(g)–(i) for the scanning area of 1.4 mm^2. The surface roughness (R_a) at the top surface of the coating is in the range of 29.85–37.73 μm.

The variations of hardness and elasticity modulus of the coating after thermal exposure were plotted in Fig. 2(j) and compared with other results of plasma sprayed coatings. The hardness and elasticity modulus of bulk YSZ material is chosen 15 GPa and 200 GPa [23], respectively. For the as-sprayed fresh coating in this work, the value of mean hardness is greater than other results by using conventional APS methods of lamellar structures and vertical cracks structure or SPS method. The measured elasticity modulus and hardness are all increased after thermal exposure for 48 h at 1473

Table 1
Comparison of experimental parameters in Fig. 1(e) and (f).

Business name	Powders	Output power	Gas flow rate	Refs.
Praxair SG-100 Torch	8YSZ, AI-1075, Praxair, US	32 kW, *I* = 800 A	Ar/He = 48/12 SLPM	[19]
Metco A -2000	8YSZ, FuJimi, Japan	40 kW, *I* = 600 A	Ar/H_2 = 35/12 SLPM	[20]
Sulzer F4VB Torch	8YSZ, Metco -204NS, US	36 kW, *I* = 600 A	Ar/H_2 = 45/15 SLPM	[21]
Triplex Pro-200 Gun	8YSZ, Metco −204NS, US	52 kW, *I* = 480−520 A	Ar = 40−50 SLPM He = 4−10 SLPM	[22]
Triplex II Gun	8YSZ, Metco −204NS, US	50 kW, *I* = 470/550 A	Ar = 40−50 SLPM He = 4 SLPM	[6]
This Work	8YSZ, Metco -204B-NS, US	25.4 kW, *I* = 160 A	N_2 /Ar = 6.3 / 2.7 SLPM	

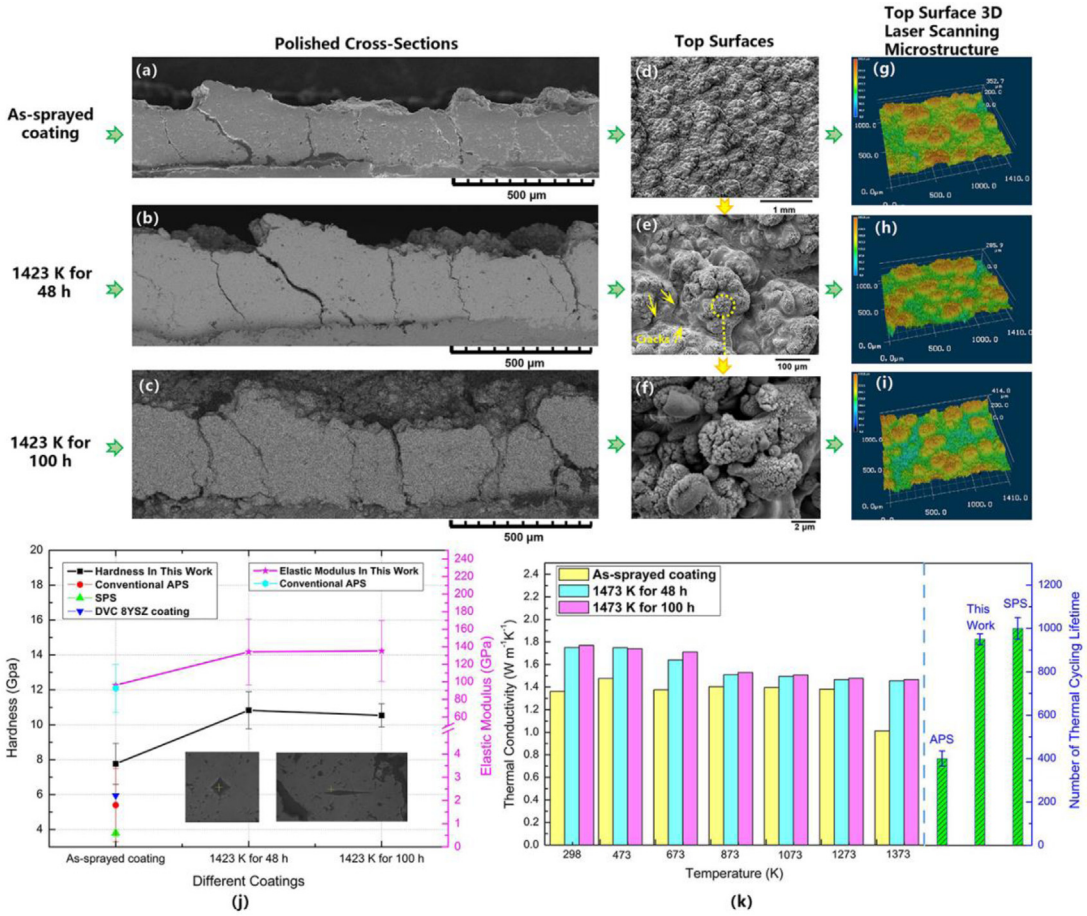

Fig. 2. The polished cross-sections of the as-sprayed coating (a), thermal exposed coatings at 1473 K for 48 h (b) and for 100 h (c); the top surface morphology of the as-sprayed coating (d), thermal exposed coatings at 1473 K for 48 h of (e) and for 100 h of (f); 3D top surface laser scanning microstructures of the as-sprayed coating (g), thermal exposed coatings at 1473 K for 48 h (h) and for 100 h (i) ; the hardness, elasticity modulus and thermal conductivity variations between the as-sprayed coating, thermal exposed coatings at 1473 K for 48 h and for 100 h are presented in (j) and (k), respectively. Also, thermal cycling lifetime were compared in (k).

K. These results varied a little after continued thermal exposure to 100 h at 1473 K. The thermal conductivity varied with the increase of temperature in the range of 1.35 W m^{-1} K^{-1} –1.0 W m^{-1} K^{-1} for the as-sprayed coating and these results rapidly increased to the maximum value of 1.75 W m^{-1} K^{-1} at the room temperature (298 K) after thermal exposure for 48 h at 1473 K. However, the distributions of thermal conductivity did not greatly vary when keep heating at 1473 K up to 100 h. Accordingly, the sintering in the YSZ coating during thermal exposure is an spontaneous process, but it was observed that the vertical cracks can not be effectively sintered in this work. Thermal barrier effect of the YSZ coating with the high density vertical cracks still work after 100 h exposure at 1473 K.

The result of thermal cycling test (furnace heating to 1150 °C for 15 min and air cooling in 5 min) in this work was shown in Fig. 2(k) and compared with other coatings by using APS method and SPS method (1121 °C for 10 min and air cooling) [17,18]. The results of this work are closed to the SPS results and higher than the result by conventional APS method (Table 2).

Electron Back-Scattered Diffraction (EBSD) analysis was performed on the cross-section of the coating in Fig. 3 with a step size of 300 nm. For the as-sprayed coating in Fig. 3(a, d, b, e), very fine grain boundaries were shown at the bottom of the coating due to a rapid solidification process when the impinging YSZ droplets flattens on the substrate at the beginning. In the experiment, the deposition rate (mm s^{-1}), mass flow rate (kg s^{-1}) and heat flux (W mm^{-2}) from the plasma jet to the substrate are all constant. Thus, the distributions of impinging droplets are almost uniform in several repeated scans of the plasma spray. Therefore, coarsened grains existed at the top layer of the coating due to the increasing of the droplets solidification time with the increasing of the coating thickness. In addition, the inter-space of the crack at the

Table 2
Experimental parameters in the manufacturing of vertical cracks of YSZ coatings.

Methods /Authors	Cracks density (mm^{-1})	Thermal conductivity ($W\ m^{-1}\ K^{-1}$)	Coating thickness (mm)	Feed power size (μm)	Spraying distance (mm)	Auxiliary heating of the Substrate	Refs.
Guo et al. (2004) by APS	0.5- 3.6	0.8–1.5	0.–1.5	39–75	70–110	Yes	[1]
Karger et al. (2011) by APS	3.5–8.9	1.4–1.8	0.3–0.5	9–51	80	Partly Yes	[27]
Jordan et al. (2014) by SPS	1–3	0.6–0.8	0.2–1.5	0.3–0.95	38–57	Partly Yes	[28,29]
This Work	4–5	0.9–1.35	0.15–0.18	39–75	270	No	

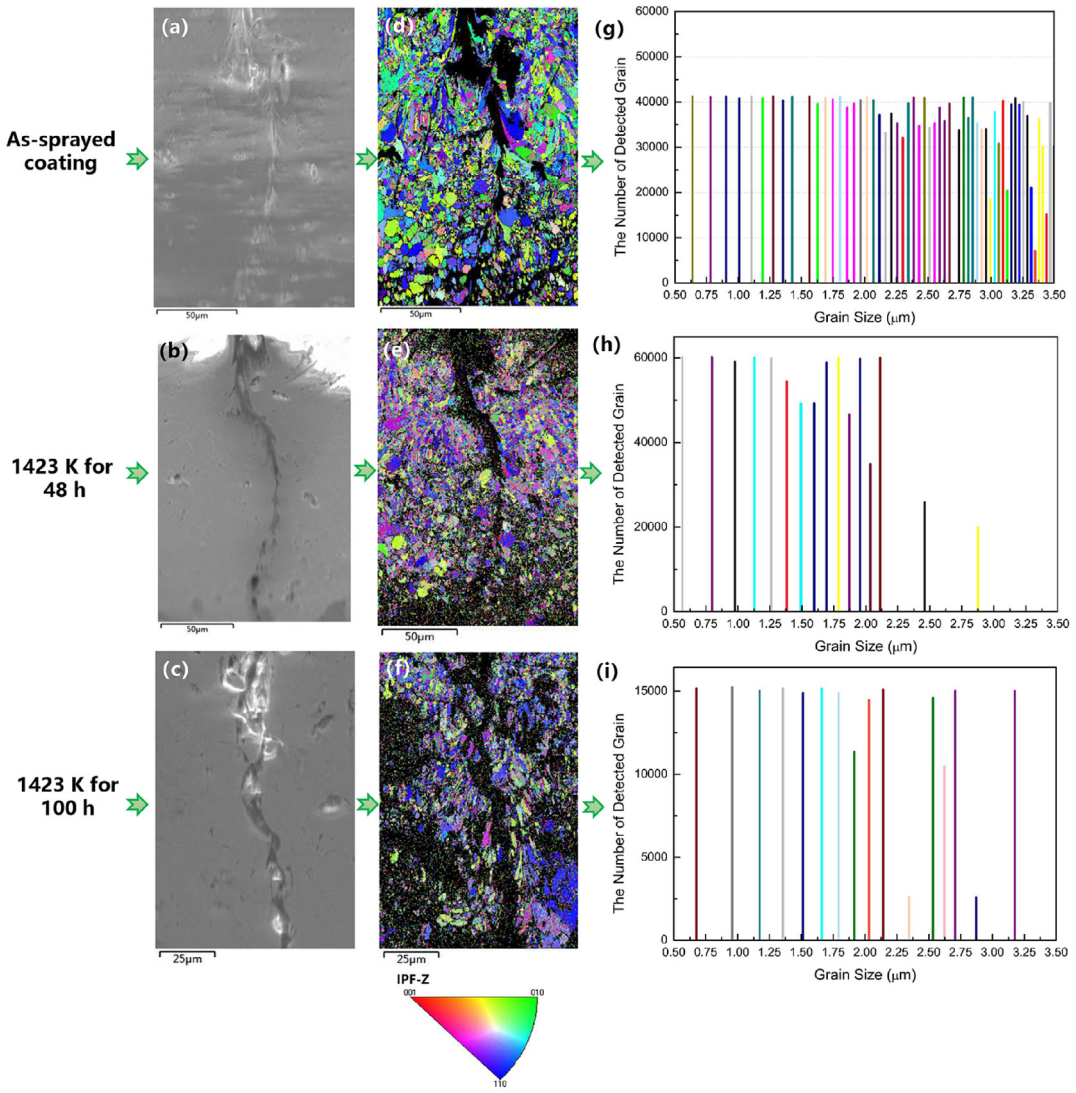

Fig. 3. EBSD analyses on the polished cross-section of the as-sprayed coating of (a), thermal exposed coatings at 1473 K for 48 h (b) and for 100 h (c); IPF-Z orientation maps between the as-sprayed coating (d), thermal exposed coatings at 1473 K for 48 h (e) and for 100 h (f); grain size distributions in the as-sprayed coating (g), thermal exposed coatings at 1473 K for 48 h (h) and for 100 h (i).

top of the coating is larger than it at the bottom of the coating, which means the vertical crack is hard to propagate at the fine grain area.

After thermal exposure at 1473 K for 48 h and up to 100 h, an apparently vertical crack still exists at the cross-section of the coating (Fig. 3(b) and (c)). The statistical results of the grain size distribution were plotted in Fig. 3(g–i). Multi-grain sizes in the range of 0.5 μm–3.5 μm were found in the as-sprayed coating and the grain size distributions were slightly decreased after thermal exposure at 1473 K for 48 h and up to 100 h.

Coupled grain-boundary diffusion and surface diffusion of grain-boundary migration are recognized as the mechanism for densification during thermal exposure [24,25]. The driving force is described as [26],

$$\Delta G = \Delta G_S + \Delta G_i = \gamma_s dA_S + \gamma_i dA_i$$

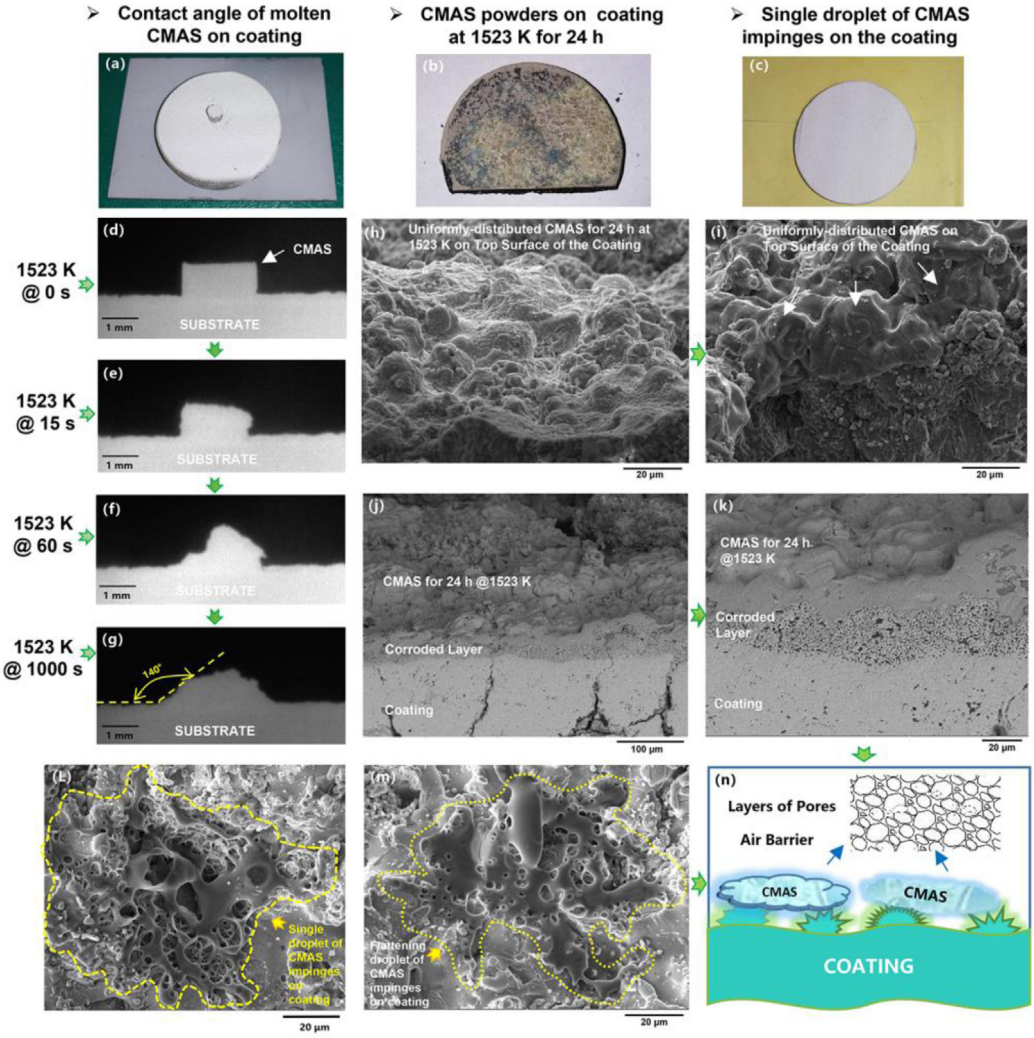

Fig. 4. Experimental samples of CMAS on top surface of coating in (a), (b), (c); In-situ observations of a sequence of states of CMAS on the surface of the coating in (d), (e), (f), (g); uniformly distributed CMAS powders at 1523 K for 24 h on the top surface of the coating in (h), (i) and on the polished cross-section of the coating (j), (k); single droplet of the CMAS impinges on the surface of the coating (L), (m) ; the schematic diagram of the molten CMAS contacting on the top micro-nano protuberances of the coating (n).

where ΔG, ΔG_s, and ΔG_i are the changes of the total free energy, surface energy, and the interface energy, γ_s and γ_i are the surface and interface tension, and A_s and A_i are the specific surface and interfacial areas, respectively. The sintering potential and the densification rate all depend on the pore size and the time.

Therefore, without external pressure in the thermal exposure, the internal pores and voids at the bottom of the coating cannot be vented and were impeded the migration of the grain boundaries. At the same time, the grain boundaries prefer to migrate at the dense layer of the coating during long time high temperature exposure.

CMAS corrosion on the top surface of the coating were studied through three different experiments in Fig. 4. In-situ observations (Fig. 4(a)) of CMAS droplet spreading on the top surface of the coating at 1523 K were listed from Fig. 4(d–g). When the CMAS bulk materials with a diameter of 2 mm melting on the surface of the coating, the finally contact angle is about 40°and the molten CMAS (viscosity of 36.7 Pa s at 1266°C [30]) cannot spread completely on the surface of the YSZ coating. The CMAS loading of about 50 mg cm^{-2} was put uniformly on the surface of the coating and then put in the muffle furnace at 1523 K for 24 h to investigate the corrosion behavior on the coating (Fig. 4(b)). The results were shown in Fig. 4(h) and (i), the CMAS were deposited on the multi-islands protrusions from the observation on the top surface. The thickness of the corroded layer with more pores is about 20–25 μm at the polished cross-section of the coating, which is less than other result of 100–150 μm corroded layer of YSZ coating at the same conditions [31,32]. The top multi-islands protrusion with a mean surface roughness (R_a) of 33.8 μm effectively hindered the spreading and penetrating of the CMAS.

Furthermore, in order to simulate the actually molten CMAS powders (from sand, debris, fly ash, and volcanic ash) impinging on the thermal barrier coating of the gas engine, we injected the CMAS powders (diameter of 5–50 μm) on the top surface of the YSZ coating by using a conventional APS method (GP-80, Jiujiang, China, 39 kW, Argon of 45 SLPM, spray distance of 100 mm) in Fig. 4(c). The morphology of single droplet impinging on the coating was shown in Fig. 4(L) and (m). An air barrier with layers of the pores was formed when the droplet of CMAS impinged on the top surface of the coating (Fig. 4(n)). The micro-sized island protrusions with nano-sized villous structures on the top surface of the coating were further hindered the flattening of the CMAS droplet. When a mass of CMAS crystalline ashes impinge on the YSZ coating of the gas engine, its molten droplets may wet on the top or on the interspace of multi-islands protrusions and form layers of multi-pores at the interface in the beginning. Then, CMAS will dissolve with the

YSZ materials and penetrate further by overcoming the internal air barrier of layers of the pores.

4. Conclusions

To summarize, the hybrid structure YSZ coating with vertical cracks at the cross-section and multi-islands protrusions at the top surface is directly deposited by using a long laminar plasma spray technology without any auxiliary heating of the substrate. The density of vertical cracks of the coating at the cross-section is 4 or 5 per millimeter. The surface roughness of R_a on the top surface of the coating is in the range of 29.85–37.73 μm. The vertical cracks in the coating cannot be sintered to a dense layer during thermal exposure at 1473 K up to 100 h. The vertical crack is hard to propagate at the fine grain area of the coating. The micro-sized island protrusions with nano-sized villous structures were hindered the spreading and penetrating of molten CMAS ashes corrosion on the top surface of the coating. The thickness of the corroded layer with more pores by CMAS is about 20−25 μm at 1523 K for 24 h. This novel hybrid structure YSZ coating may provide a new selection for various working environments of higher-temperature thermal barrier coatings of aircraft propulsion or land-based electricity generation and this deposition process significantly improved the working environment of workers.

Acknowledgements

This work was financially supported by the National Key R&D Program of China (Basic Research Project, No. 2017YFB0306104), National Natural Science Foundation of China (Nos. 91860114, 51590894 and 51901011), the China Postdoctoral Foundation and National Science and Technology Major Project (No. 2017-VI-0010-0081).

References

[1] H.B. Guo, R. VaEn, D. StVer, Surf. Coat. Technol. 186 (2004) 353–363.
[2] R. VabEn, H. KaNer, G. Mauer, D. StVer, J. Therm. Spray Technol. 19 (2010) 219–225.
[3] P. Fauchais, M. Vardelle, A. Vardelle, S. Goutier, J. Therm. Spray Technol. 24 (2015) 1120–1129.
[4] B. Bernard, A. Quet, L. Bianchi, V. Schick, A. Joulia, A. Malié, B. Rémy, J. Therm. Spray Technol. 26 (2017) 1025–1037.
[5] P.L. Fauchais, J.V.R. Heberlein, M.I. Boulos, Thermal Spray Fundamentals, Springer Science+Business Media, 2014.
[6] P. Fauchais, A. Joulia, S. Goutier, C. Chazelas, M. Vardelle, A. Vardelle, S. Rossignol, J. Phys. D-Appl. Phys. 46 (2013) 224015.
[7] G. Mauer, V. Robert, S. Detlev, Surf. Coat. Technol. 202 (2008) 4374–4381.
[8] J.P. Trelles, E. Pfender, J. Heberlein, IEEE Trans. Plasma Sci. 36 (2008) 1026–1027.
[9] M. Baeva, D. Loffhagen, M.M. Becker, D. Uhrlandt, Plasma Chem. Plasma Process. 39 (2019) 949–968.
[10] C.X. Li, S.H. Liu, C.J. Li, L. Li, J.H. Huang, P. Xu, China Surf. Eng. 32 (2019) 1–19 (In Chinese).
[11] S.H. Liu, S.L. Zhang, C.X. Li, L. Li, J.H. Huang, J.P. Trelles, B. Anthony, C.L. Murphy, Plasma Chem. Plasma Process. 39 (2019) 377–394.
[12] S.H. Liu, C.X. Li, L. Li, J.H. Huang, P. Xu, Y.Z. Hua, G.J. Yang, C.J. Li, Surf. Coat. Technol. 337 (2018) 241–249.
[13] S.H. Liu, J.P. Trelles, C.J. Li, H.B. Guo, C.X. Li, J. Phys. D-Appl. Phys. 53 (2020) 375202.
[14] S.H. Liu, C.X. Li, H.Y. Zhang, S.L. Zhang, L. Li, P. Xu, G.J. Yang, C.J. Li, Scr. Mater. 153 (2018) 73–76.
[15] S.H. Liu, H.Y. Zhang, Y.P. Wang, G. Ji, L. Li, P. Xu, J.H. Huang, S.L. Zhang, C.X. Li, C.J. Li, Surf. Coat. Technol. 363 (2019) 210–220.
[16] Standard Test Method for Thermal Diffusivity by the Flash Method, ASTM E1461–07, 2007 http://www.astm.org/DATABASE.CART/HISTORICAL/E1461-07.htm.
[17] Y. Wang, H. Guo, S. Gong, Ceram. Int. 35 (2009) 2639–2644.
[18] S.H. Liu, J.P. Trelles, A.B. Murphy, L. Li, S.L. Zhang, G.J. Yang, C.X. Li, C.J. Li,J. Phys. D-Appl. Phys. 52 (2019), 335203.
[19] L. Vincenzi, S. Suzuki, D. Outcalt, J. Heberlein, Controlling spray torch fluid dynamics—effect on spray particle and coating characteristics, J. Ther. Spray Technol. 19 (4) (2010) 713–722.
20 C. Zhang, H.L. Liao, W.Y. Li, G. Zhang, C. Coddet, C. Zhang, et al., Characterization of ysz solid oxide fuel cells electrolyte deposited by atmospheric plasma spraying and low pressure plasma spraying, J. Ther. Spray Technol. 15 (4) (2006) 598–603.
21 V. Debout, A. Vardelle, P. Fauchais, E. Meillot, E. Bruneton, F. Enguehard, S. Schelz, High Temp. Mater. Proc. 11 (2007) 309–320.
22 G. Mauer, R. VapEn, D. StVer, Surf. Coat. Technol. 204 (1-2) (2009) 172–179.
[23] D. Basu, C. Funke, R.W. Steinbrech, J. Mater. Res. 14 (1999) 4643–4650.
[24] J. Pan, H.N. Ch'Ng, A.C.F. Cocks, Mech. Mater. 37 (2005) 705–721.
[25] J.L. Shi, J. Mater. Res. 14 (4) (1999).
[26] R.M. German, Crit. Rev. Solid State Mater. Sci. 35 (2010) 263–305.
[27] M. Karger, R. Vaßen, D. Stöver, Surf. Coat. Technol. 206 (1) (2011) 16–23.
[28] E.H. Jordan, C. Jiang, J. Roth, M. Gell, J. Ther. Spray Technol. (2014) 849–859.
[29] M. Gell, E.H. Jordan, M. Teicholz, B.M. Cetegen, N.P. Padture, L. Xie, D. Chen, J. Ther. Spray Technol. (2008) 124–135.
[30] V.L. Wiesner, U.K. Vempati, N.P. Bansal, Scripta Mater. 124 (2016) 189–192.
[31] T. Liu, S.W. Yao, L.S. Wang, G.J. Yang, C.X. Li, C.J. Li, J. Ther. Spray Technol. 25 (1-2) (2016) 213–221.
[32] J.M. Drexler, K. Shinoda, A.L. Ortiz, D. Li, A.L. Vasiliev, A.D. Gledhill, et al., Acta Mater 58 (20) (2010) 6835–6844.

Sen-Hui Liu
School of Materials Science and Engineering, Beihang University, Beijing, 100191, China

Gang Ji
Chang-Jiu Li
Cheng-Xin Li*
School of Materials Science and Engineering, Xi'an Jiaotong University, Xi'an, 710049, China

Hong-Bo Guo**
School of Materials Science and Engineering, Beihang University, Beijing, 100191, China

* Corresponding author at: School of Materials Science and Engineering, Xi'an Jiaotong University, State Key Laboratory for Mechanical Behavior of Materials, Xi'an, Shaanxi, 710049, China.

** Corresponding author at: School of Materials Science and Engineering, Beihang University, Key Laboratory of Aerospace Materials and Performance (Ministry of Education), Beihang University, No. 37 Xueyuan Road, Beijing, 100191, China.
E-mail addresses: licx@xjtu.edu.cn (C.-X. Li), guo.hongbo@buaa.edu.cn (H.-B. Guo).

31 March 2020